Chinese Journal of Chemical Engineering 69 (2024) 72–78

Contents lists available at ScienceDirect

Chinese Journal of Chemical Engineering

journal homepage: www.elsevier.com/locate/CJChE

Full Length Article

Facile molybdenum and aluminum recovery from spent hydrogenation catalyst

Zhenhui Lv [1, 2, #], Jianan Li [1, #], Dong Xue [2], Tao Yang [2], Gang Wang [2], Chong Peng [1, *]

[1] State Key Laboratory of Fine Chemicals, School of Chemical Engineering, Dalian University of Technology, Dalian 116024, China
[2] Dalian Research Institute of Petroleum and Petrochemicals, SINOPEC, Dalian 116041, China

ARTICLE INFO

Article history:
Received 1 August 2023
Received in revised form
20 January 2024
Accepted 21 January 2024
Available online 17 February 2024

Keywords:
Waste treatment
Alumina
Hydrogenation
Catalyst
Crystallization
Precipitation

ABSTRACT

Industrial catalyst waste has emerged as a hazardous pollutant that requires safe and proper disposal after the unloading process. Finding a valuable and sustainable strategy for its treatment is a significant challenge compared to traditional methods. In this study, we present a facile method for the recovery of molybdenum and aluminum contents from spent Mo–Ni/Al_2O_3 hydrogenation catalysts through crystallization separation and coprecipitation. Furthermore, the recovered molybdenum and aluminum are utilized as active metals and carriers for the preparation of new catalysts. Their properties were thoroughly analyzed and investigated using various characterization techniques. The hydrogenation activity of these newly prepared catalysts was evaluated on a fixed-bed small-scale device and compared with a reference catalyst synthesized from commercial raw reagents. Finally, the hydrogenation activity of the catalysts was further assessed by using the entire distillate oil of coal liquefaction as the raw oil, specifically focusing on denitrogenation and aromatic saturation. This work not only offers an effective solution for recycling catalysts but also promotes sustainable development.

1. Introduction

Catalysts play a crucial role in the petroleum refining process and are used in substantial quantities [1,2]. However, as the reaction progresses, their activity and selectivity gradually decrease due to various factors, such as carbon deposition and poisoning [3]. Once their performance no longer meets the production requirement, they are unloaded from the device and discarded as solid waste. It is important to note that the unloaded spent catalysts often contain toxic and harmful metal elements, such as nickel and vanadium, in oxidized states. Improper disposal can lead to the conversion of these elements into ions that enter the water and soil, causing pollution in the ecological system. The conventional methods of deep burial or incineration not only harm the environment but also overlook the potential of catalyst waste as a new metal resource [4]. For instance, in the case of waste catalysts from oil refining hydrogenation, it has been reported that approximately 500000–700000 tons of metals are discarded annually worldwide. Despite the significant quantity of metals involved in refining catalyst processing, their recovery has not received sufficient attention in the past [5]. Therefore, in order to minimize the loss of metal resources and prevent serious environmental pollution, numerous strategies have been proposed to efficiently recycle waste refining catalysts.

Hydrodesulfurization (HDS) catalysts are the most commonly used catalysts in the petroleum and chemical industries [6,7]. Typically composed of active components such as molybdenum, cobalt, nickel, and alumina as the carriers, a significant amount of metal substances in spent HDS catalysts can be efficiently separated and recovered compared to direct discharge as hazardous waste [8,9]. Various methods, including acid or alkali leaching, have been attempted to recover metals from spent catalysts. For example, ultrasonic-assisted acid leaching has been employed to extract valuable metals such as Mo, V, and Ni from spent hydroprocessing catalysts [10,11]. Another novel process, including alkali hydrothermal treatment, sulfuric acid washing, and calcination, has been conducted to recover anatase TiO_2 from spent catalysts [12]. Sulfuric and nitric acid solutions have also been used to extract molybdenum and cobalt from spent Co–Mo/Al_2O_3 catalysts [13]. However, several challenges still exist, including limited recycling contents, low recovery efficiency, and refractory leaching solutions [14]. Therefore, there is a strong need for more effective strategies to enhance the separation and recovery processes of metals in

* Corresponding author.
E-mail address: pengchong@dlut.edu.cn (C. Peng).
# These authors contributed equally to this work.

https://doi.org/10.1016/j.cjche.2024.01.006
1004-9541/

spent hydrogenation catalysts. Considering environmental sustainability, it is necessary to utilize this abundant solid waste to generate marketable products, such as new catalysts.

Herein, we employed a strategy of crystallization separation and coprecipitation to recover molybdenum oxide and alumina from the spent Mo–Ni/Al_2O_3 waste hydrogenation catalysts. Furthermore, the recovered molybdenum and aluminum could be used as raw materials for active metals and carriers in the preparation of new catalysts. Through comprehensive analysis, the crystal phase and pore structure of the recovered samples were presented and compared. In addition, the recovered molybdenum and aluminum were used to resynthesize a new Mo–Ni/Al_2O_3 catalyst. The catalytic hydrogenation activity of these newly prepared catalysts was also evaluated using the entire distillate oil of coal liquefaction, focusing on denitrogenation and aromatic saturation. The separation and recycling of metal substances can promote resource recycling within the entire enterprise and ensure its sustainable development.

2. Experimental

2.1. Chemical and materials

All of the reagents (analytical grade) in this work were purchased from Sinopharm Chemical Reagent Co., Ltd., China. The spent Mo–Ni–Al_2O_3 catalysts were obtained from industrial unloading. The commercial support was employed as the reference for comparison. Ultra-pure deionized (DI) water (>18 MΩ·cm^{-1}) was produced from a Milli-Q system and used to prepare the various required solutions.

2.2. Recycling of spent Mo–Ni–Al_2O_3 catalyst

2.2.1. Molybdenum recovery

The spent Mo–Ni–Al_2O_3 catalysts from industrial unloading were extracted in a mixed solution of petroleum ether and ethanol for 48 h to remove the residue oil. After that, the catalysts were further dried in the oven and consequently calcinated to remove the carbon deposition on the surface. Then, the obtained deoiling and decarburization catalysts were ground to 80–120 mesh (0.12–0.18mm) and added to the Na_2CO_3 solution in the autoclave reactor with a mass ratio of 1:0.7. Through a hydrothermal reaction at 150 °C for 2.5 h, the nickel- and aluminum-rich residue and molybdenum-containing solution were obtained separately by simple filtration. By adding NH_4Cl to the obtained molybdenum-containing solution and adjusting the pH value within 1–2, the molybdenum acid (H_2MoO_4) crystals will appear from the solution and be separated by filtration.

2.2.2. Alumina carrier recovery

The above-obtained nickel and aluminum-rich residues are mixed evenly with Na_2CO_3 according to a certain ratio. Then, this mixture was roasted at a high temperature of 800–900 °C. The roasted solid was dissolved in water by continuous stirring and subsequently filtered to obtain a crude sodium meta-aluminate solution. After a deep purification, the required quality of meta-aluminate sodium solution could be achieved. Sodium meta-aluminate and aluminum sulfate are neutralized in the formation of a gel to prepare the required macro-porous pseudo-boehmite. The prepared pseudo-boehmite is mixed, kneaded in the extruder, and extruded into the required carrier precursor. The alumina carrier could be acquired from the carrier precursor after drying and roasting.

2.2.3. Preparation of new Mo–Ni–Al_2O_3 catalyst

The molybdic acid and nickel nitrate obtained from the recovery treatment were dissolved in the ammonia to form a mixed solution of ammonium molybdate and nickel nitrate. Then, Al_2O_3 carriers were impregnated completely in this mixture solution. Finally, the obtained precursors were dried and roasted to regenerate a new Mo–Ni/Al_2O_3 catalyst. As a comparison, the reference catalyst was also prepared with the same procedure, but commercial ammonium molybdate, nickel nitrate, and Al_2O_3 carriers were employed in the preparation process.

2.3. Characterizations

X-ray fluorescence (XRF) was carried out on ARL Quant'X (Thermo Fisher Scientific, USA) in vacuum. X-ray diffraction (XRD) was carried out on a D/Max-2400 (Rigaku Corporation, Japan) with Cu K_α radiation (λ = 0.15418 nm) at a scan rate of 1 (°)·min^{-1}. Raman spectra were recorded on a DXR3 Raman Microscope (Thermo Fisher Scientific, US) by using the laser at 532 nm. The infrared spectroscopy of CO adsorption was put forward on a Chemisorption-300 AUTOSORB-I-C chemisorption measurement (Quantachrome Instruments, US). The catalysts were first pretreated at 200 °C for 1 h to remove the adsorbed water before weighing. Then, the samples were pretreated in a hydrogen atmosphere at 300 °C for another 2 h, and their CO adsorption abilities were measured at 35 °C. X-ray photoelectron spectroscopy (XPS) was conducted on a MULTILAB 2000 spectrometer (Thermo Fisher Scientific, US) with an X-ray source of Al K_α to characterize the surface chemical status of catalyst samples. Specially, the obtained results were calibrated by the C 1s binding energy at 284.6 eV. The specific surface area and pore information of catalyst samples were determined by the Brunauer-Emmett-Teller (BET) method using the apparatus ASAP 2405 physical adsorption analyzer (Micromeritics Inc., USA). A scanning electron microscope (SEM) was conducted on the HITACHI S4800 to observe the micromorphology. High-resolution transmission electron microscopy (HR-TEM) was conducted on a JEM-2100 plus transmission electron microscope (JEOL Ltd., Japan). The average slab length (L) and average stacking layer number (N) of MoS_2 were estimated according to Eqs. (1) and (2):

$$L = \frac{\sum_{i=1}^{n} S_i L_i}{\sum_{i=1}^{n} S_i} \tag{1}$$

$$N = \frac{\sum_{i=1}^{n} S_i N_i}{\sum_{i=1}^{n} S_i} \tag{2}$$

where L_i represents the sheet length of a MoS_2, N_i represents the stacking layer number of a MoS_2 unit, and S_i is the number of slabs or stacks in a determined range of length or stacking layer number.

2.4. Catalysis activity evaluation

In order to better reflect the performance of the active catalyst in the reaction, a vulcanization pretreatment of the catalyst was carried out to convert these oxides into sulfides before catalytic activity evaluation. The vulcanization of the catalyst was prepared on a fixed-bed automatic control micro-reactor. *n*-Dodecane dissolved in dimethyl disulfide was regarded as the vulcanized oil, and the vulcanization process took place by a two-stage temperature

control, respectively 230 °C for 4 h and 340 °C for 3 h (pressure = 4.0 MPa, hydrogen-oil volume ratio = 500:1).

The catalyst performance evaluations were carried out on a fixed-bed, small-scale device. The upper and lower sections of the reactor were filled with quartz sand, while the middle part, keeping a constant temperature, was filled with the grounded catalyst (16–22 mesh, 0.72–1.00 mm). The whole catalyst loading volume was about 80 ml. The jet fuel with dimethyl disulfide dissolved was employed as the vulcanized oil in the examination, and the vulcanization process was carried out through a temperature control on both ends at 230 °C and 340 °C for 8 h to vulcanize the catalyst.

3. Results and Discussion

3.1. Schematic illustration of Mo–Ni/Al_2O_3 recovery treatment

The recovery treatment procedure of the spent Mo–Ni/Al_2O_3 catalyst could be divided into three sections (Fig. 1 and Fig. S1). These sections include: (1) the pretreatment section; (2) the recovery section; and (3) the resynthesis section. In the pretreatment section, the unloaded hydrogenation catalysts (Sample #B) underwent roasting at temperatures ranging from 200 to 500 °C. This roasting process aimed to eliminate carbon, hydrogen, sulfur, nitrogen, and other impurities in the spent catalyst. After roasting, the carbon content in the catalyst (Sample #C) was reduced to less than 1%. The catalyst was then ground into 80–120 mesh (0.12–0.18 mm) powder (Sample #D) before being mixed with a leaching agent, Na_2CO_3 solution, at a ratio of 1:0.7. The mixture was transferred into an autoclave reactor to induce the hydrothermal leaching of Mo contents under mild conditions of 150 °C for 2.5 h. Notably, the strategy prevented the dissolution of aluminum and nickel metal by Na_2CO_3, ensuring only molybdenum was dissolved in the solution at low temperatures [15,16]. This safeguarded the purity of the subsequent recovery ingredients. Moreover, the relatively low temperature of hydrothermal treatment prioritized the high-temperature process. It prevented the volatilization of molybdenum and the crystal transformation of aluminum, which could affect the subsequent recovery efficiency [16]. After the hydrothermal reaction, the solid and liquid were separated, yielding the Mo-containing solution (Sample #H) and the first treated catalyst (Sample #E). On one side, a precipitating agent was added to the Mo-containing solution with pH regulation. This conversion converted molybdenum salt into molybdenum acid, forming crystals and precipitates. By means of crystallization and filtration, the residual liquid (Sample #J) and polymolybdic acid products (Sample #I) were separated and obtained. On the other side, the first treated catalyst was mixed with Na_2CO_3 to induce an aluminum-dissolving reaction at high temperatures (800–900 °C). Notably, Na_2CO_3 reacted with aluminum to generate sodium meta-aluminate and carbon dioxide. The former was soluble in water and easily separated [17,18]. After that, the supernatant (Sample #K) consisted of crude sodium meta-aluminate solution with nickel-rich residue (NiO content >60%) (Sample #G). The obtained crude sodium meta-aluminate was further purified through a hydrothermal reaction to obtain a refined sodium meta-aluminate solution and waste residue. In this process, the refined sodium meta-aluminate solution and aluminum sulfate were added into an autoclave containing a certain amount of bottom water. They were neutralized and reacted at temperatures ranging from 20 to 100 °C for 0.5–5 h. The pseudoboehmite products (Sample #M) were obtained from the reaction effluent and regarded as a raw material for the alumina carrier (Sample #N). Finally, the new Ni–Mo/Al_2O_3 catalyst (Sample #A') was resynthesized by the impregnation method using Samples #I and #N. The active metal atomic ratio of Mo and Ni was optimized in this process [19,20]. Compared to conventional recovery methods, this facile strategy enables the sequential separation of metal components under relatively mild

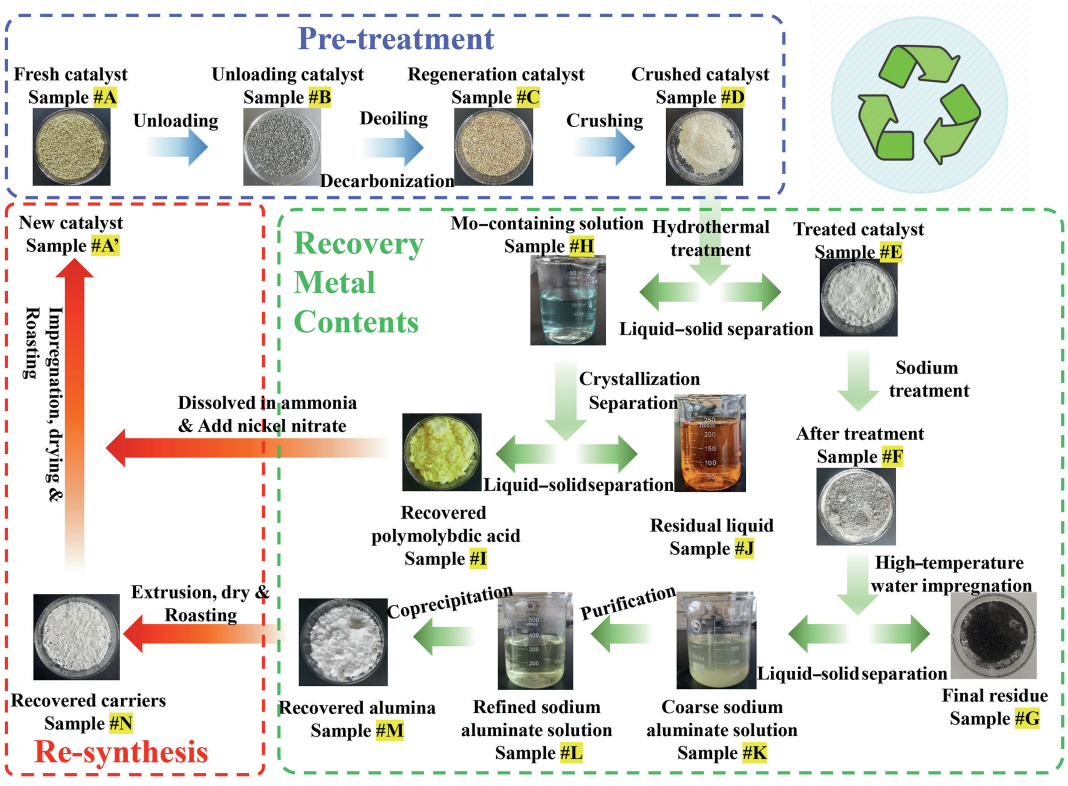

Fig. 1. Illustration of Mo–Ni/Al_2O_3 recovery treatment process.

conditions, greatly increasing the potential for waste-to-wealth conversion.

3.2. Sample analysis during Mo–Ni–Al_2O_3 recovery treatment

The main components of the obtained substances from each procedure were initially analyzed by X-ray fluorescence (XRF) technology (Table 1). Analysis revealed that Sample #D was predominantly consisted of Al_2O_3 (57.61% (mass)) and MoO_3 (20.43% (mass)). Subsequent hydrothermal treatment led to a significant decrease in MoO_3 content in Sample #E, down to 1.36% (mass), while the Al_2O_3 content increased to 87.05% (mass), indicating effective separation of the molybdenum component. Both Samples #D and #E maintained similar NiO content, suggesting negligible changes in the nickel content during the special hydrothermal treatment. The final Sample #G, primarily consisted of NiO (68.6% (mass)) with a small amount of remaining Al_2O_3 and Na_2O left. Additionally, the recovered polymolybdic acid (Sample #I) contained MoO_3 at a purity level of nearly 88.52% (mass), which is sufficient to meet commercial standards. The recovered alumina (Sample #M) mainly comprised high-purity Al_2O_3 (97.07% (mass)) with relatively low levels of other metal impurities. These findings indicate that the metal contents can be successfully recovered from the spent Mo–Ni/Al_2O_3 catalyst, thus demonstrating the feasibility of this method.

In addition, the crystal phase of these substances obtained from the spent Mo–Ni/Al_2O_3 catalysts was determined through XRD analysis (Fig. 2). After the hydrothermal treatment, the Mo-containing solution and treated catalysts were separated. The XRD patterns of first-treated catalysts still showed peaks corresponding to γ-Al_2O_3 (JCPDS No. 04-0880) at 37.27°, 39.5°, 46.0°, 60.4°, and 67.0°, and to NiO (JCPDS No. 44-1159) at 62.88° (Fig. 2(a)) [21,22]. Some MoO_3 species remained, as indicated by the peaks at 16.5°, 28.4°, 48.9°, 50.0°, and 56.3° (JCPDS No. 21-0569), which were more difficult to remove. By adjusting the pH to induce the crystallization separation, polymolybdic acid (Sample #I) was obtained, although it lacked well-defined crystallinity (Fig. 2(b)). The broad diffraction peaks observed mainly suggested a coarse crystal state, with a small amount of ammonium polymolybdate possibly resulting from the crystallization separation process. The final residue, referred to as Sample #G, consisted primarily of NiO, as indicated by the diffraction peaks at 37.27°, 43.27°, and 62.88° corresponding to (1 1 1), (2 0 0), and (2 2 0) crystal planes (JCPDS No. 47-1049), respectively (Fig. 2(c)). Additionally, the alumina (Sample #M) was recovered from the coarse sodium aluminate solution after purification. The XRD patterns of Sample #M (Fig. 2(d)) confirmed the presence of γ-Al_2O_3, with characteristic peaks at 2θ = 37.5°, 39.5°, 46.0°, and 67.0° corresponding to the (3 1 1), (2 2 2), (4 0 0), and (4 4 1) crystal planes (JCPDS No. 04-0880), respectively. These XRD patterns provided evidence of the successful recovery treatment and the attainment of the desired target products.

Furthermore, the morphology of these substances obtained from each recovery section was characterized using SEM techniques (Fig. S2). Upon calcination and crushing, the catalyst Sample #D predominantly exhibited a particle shape with a metal coating (Fig. S2(a)). However, as a result of the hydrothermal treatment, some metals within catalyst Sample #E may have been dissolved (Fig. S2(b)), exposing the internal alumina particles prominently. This observation provides evidence for the effectiveness of the separation treatment, wherein active metal components were removed from the alumina carriers. Additionally, the obtained polymolybdic acid (Sample #I) displayed a unique crystal structure (Fig. S2(c)), albeit with relatively low crystallinity. The recovered alumina (Sample #O) exhibited a porous structure, while the final residue (Sample #G) mainly consisted of accumulated NiO particles (Fig. S2(d)-(e)).

3.3. Mo–Ni/Al_2O_3 regeneration

The pore structures of recovered alumina (Sample #M), reprepared supports (Sample #N), re-synthesized Mo–Ni/Al_2O_3 catalysts (Sample #A'), and reference Mo–Ni/Al_2O_3 catalysts (Sample #R) were compared using N_2 adsorption-desorption measurements (Fig. S3(a)). It is important to note that Sample #R was prepared using the same method as Sample #A', except for the use of commercial reagents as raw materials. According to the summary in Table S1, Sample #M exhibited a large specific surface area and pore volume. The alumina carrier (Sample #N) was obtained by extrusion molding a mixture of nitric acid and Sample #M, followed by drying and roasting. The obtained molybdic acid, nickel nitrate, and ammonia water were then dissolved together to impregnate the alumina carriers (Sample #N) and reprepare the Mo–Ni/Al_2O_3 catalyst, which showed similar porous structure properties to the reference catalyst. The proportion of pore volume (pore size of <8 nm) to total pore volume was equivalent in these two Mo–Ni/Al_2O_3 catalysts. However, the proportion of pore volume (pore size in the range of 8–15 nm) to total pore volume was greater in the reprepared catalyst, while the reprepared catalyst had a slightly smaller proportion (pore size >15 nm) compared to the reference one (Table S2). The distribution of pore structure between the carrier and the catalyst indicated that the microstructure of the recycled catalyst is similar to that of the fresh one.

The XRD analysis results showed the recovered alumina exhibited typical characteristics of the γ-Al_2O_3 crystal phase (JCPDS No. 04-0880) (Fig. 3(a)), whose characteristic peaks are at 37.5°, 39.5°, 46.0°, and 67.0°, respectively. These results confirmed that the γ-Al_2O_3 carrier remained unchanged and no nickel aluminum spinel phase was formed regardless of the preparation method. It is worth noting that the characteristic peak at 58.4° corresponds to

Table 1
XRF analysis of the obtained substance in the recovery process

Substance	Content/% (mass)				
	Sample #D	Sample #E	Sample #I	Sample #G	Sample #M
Na_2O	1.67	0.06	0.49	5.05	–
Al_2O_3	57.61	87.05	0.02	8.63	97.07
SiO_2	0.80	0.35	0.03	0.16	0.84
P_2O_5	2.91	3.95	0.21	0.77	0.09
SO_3	9.65	0.15	0	0.01	1.55
CaO	0.54	0.11	0.37	1.51	0.02
Fe_2O_3	0.62	0.35	0.14	4.41	0.03
NiO	5.41	6.46	0.02	68.60	0.01
MoO_3	20.43	1.36	–	0.18	0.23
H_2MoO_4	–	–	98.52	–	–

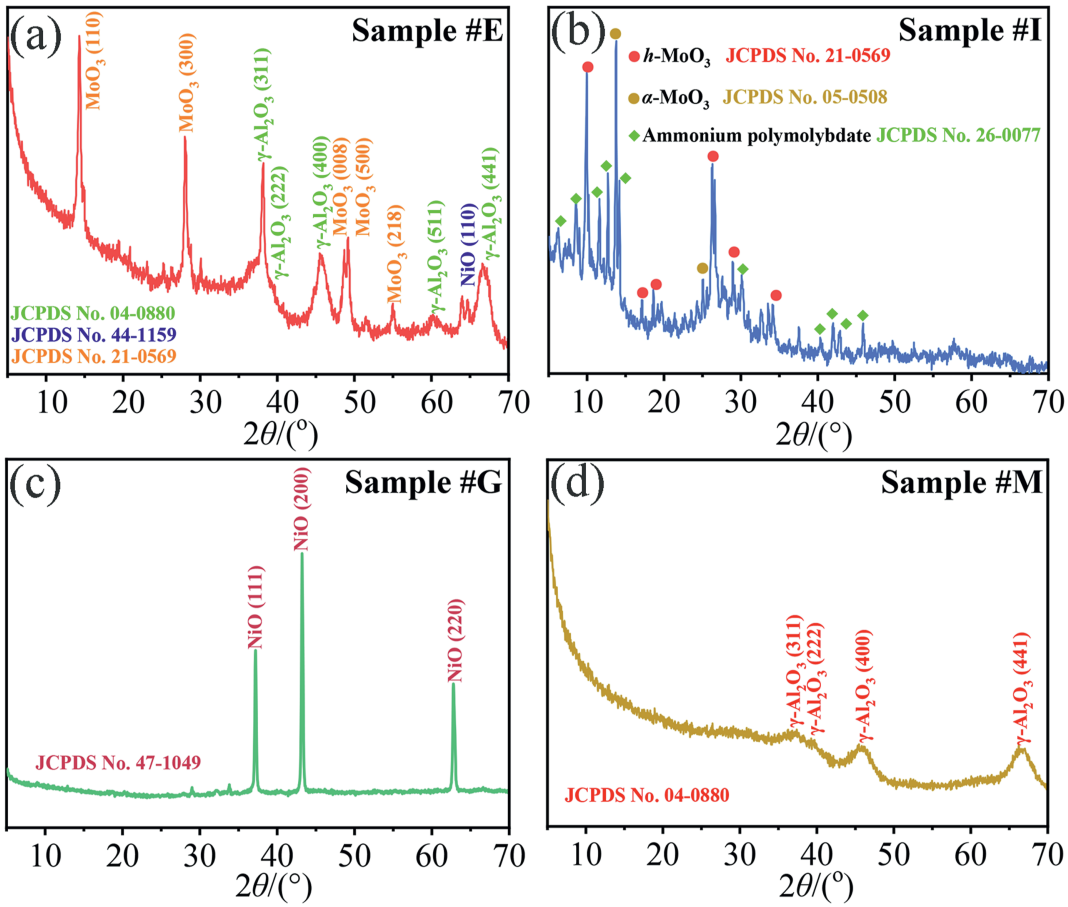

Fig. 2. XRD patterns of (a) first treated catalysts, (b) polymolybdic acid, (c) final residue, and (d) alumina obtained during recovery treatment.

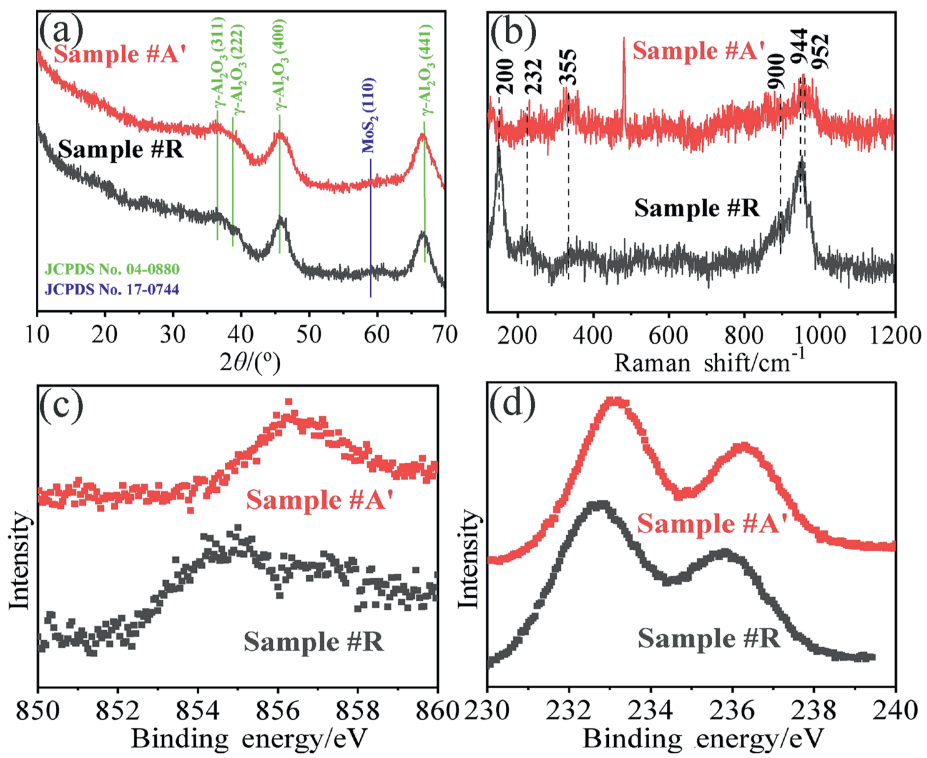

Fig. 3. The comparison of resynthesized catalysts and referred one in (a) XRD patterns, (b) Raman spectra, high-resolution XPS spectra of (c) Mo 3d and (d) Ni 2p orbits.

the MoS_2 phase formed (JCPDS No. 17-0744) during the vulcanization process.

To investigate the surface states, Sample #A' and #R catalysts were characterized by the CO adsorption infrared spectrum (CO-IR) (Fig. S3(b)). The infrared spectra of CO-adsorption of the two catalysts showed similarities. Specifically, the peaks at 2195 and 2156 cm^{-1} are characteristic of the interaction between CO and Al^{3+} coordinatively unsaturated sites (CUS) as well as acidic OH groups in alumina [23]. Additionally, the peak at 2120 cm^{-1} is a characteristic peak of CO adsorption on unpromoted sites without the influence of additives [24,25]. Furthermore, the peaks at 2080 and 2050 cm^{-1} are specific to CO adsorption on Ni-promoted sites [26]. These two peaks, respectively, represent the CO adsorption on Ni sites and Mo sites in the active phase of NiMoS. The combination of these peaks within 2050–2150 cm^{-1} suggests the presence of an additive characteristic peak.

The Raman characterizations of Sample #A' and #R catalysts were also carried out to study the surface states (Fig. 3(b)). The Raman signals within the ranges of 890–1000 cm^{-1} and 830–970 cm^{-1} correspond to the symmetric and asymmetric vibration of Mo=O bonds [27]. The Raman signals in the range of 310–370 cm^{-1} indicate the bending vibration of end Mo=O bonds [28]. The analysis reveals two main molybdenum oxide species, located at 350 and 950 cm^{-1}, respectively, representing the presence of the symmetric octahedron $Mo_7O_{24}^{6-}$ [29]. Additionally, the Raman scattering peaks at 225, 925, and 965 cm^{-1} are assigned to the symmetric octahedron $Mo_8O_{26}^{4-}$ [30]. The intensity of the Raman peaks indirectly indicates the abundance of molybdate species in the catalyst. These results demonstrate that the number and strength of the active phase structure in the resynthesized catalyst from the recovered contents are comparable to those of the fresh one, highlighting the feasibility of this recovery strategy in sustainable development.

3.4. Performance evaluation

First, to investigate the impact of the valence state of active Mo and Ni species on the sulfidation degree, the vulcanized Mo–Ni/Al_2O_3 catalyst was characterized using XPS technology with high-resolution Mo 3d and Ni 2p spectra (Fig. 3(c)). The Mo 3d orbit analysis revealed the presence of sulfurized Mo^{4+} species (229.0 and 232.2 eV), weaker unsulfurized Mo^{6+} species (232.6 and 235.8 eV), and Mo^{5+} species in the form of O–Mo–S (230.7 and 233.9 eV), respectively [31]. Additionally, the Ni 2p spectrum displayed a sulfide state with a binding energy ranging from 853.3 to 856.5 eV (Fig. 3(d)) [32]. Moreover, high-resolution transmission electron microscope (HRTEM) characterization (Fig. S4) revealed that the surface of MoO_3 was converted into a typical lamellar structure of MoS_2 after vulcanization. The average slab length (L) and average stacking layer number (N) of MoS_2 were calculated based on the count in the field of view, and the results showed that they were essentially the same as those of the reference catalyst (Table S3). This further confirms that the active phase structure of the resynthesized catalyst is almost identical to that of the fresh one. These findings provide evidence that the valence and structure of the metal phase in the resynthesized catalyst from the recovered metals meet the basic characteristics of hydrogenation catalysts.

Moreover, the performance evaluation of these catalysts was carried out using a fixed-bed, small-scale device. Prior to the evaluation, the catalysts were presulfurized by a vulcanized oil containing 10% (mass) dimethyl disulfides. The catalytic activity of the hydrogenation catalysts was assessed by introducing the whole distillate oil of coal liquefaction (Table S4) as the raw feeding material into the reactor. The catalyst activity evaluation was carried out under common conditions, including a hydrogen partial pressure of 13.0 MPa, a hydrogen-to-oil volume ratio of 300:1, a reaction temperature of 370 °C, and a volume space velocity of 1.5 h^{-1}. The measurement results (Table 2) showed that the properties of refined oil obtained using the re-synthesized catalyst were similar to those obtained using the reference catalyst, with some discrepancies in certain parameters. Specifically, the nitrogen content in the refinery oil produced by the re-synthesized catalyst from the recovery metals was approximately 229 $g \cdot g^{-1}$, while that obtained using the reference catalyst was about 157 $g \cdot g^{-1}$. This indicates a slightly lower activity of the re-synthesized catalyst in removing nitrogen impurities during the hydrogenation treatment. The molar percentages of total cycloparaffins and total aromatics obtained in the refined oil from the re-synthesized catalyst were 31.8% and 64.8%, respectively, whereas the corresponding values from the reference catalyst were 37.0% and 59.7%, respectively. This suggests that the aromatic hydrocarbons in the refined oil produced by the re-synthesized catalyst were less saturated, resulting in the formation of a smaller amount of total cycloparaffins during the hydrogenation process. These results demonstrate that the re-synthesized catalysts using the recovery metal ions from the spent catalysts can exhibit similar hydrogenation activity to those using commercial raw reagents, thus highlighting the potential of valuable elements from waste catalyst. Such a strategy for the cycling utilization of spent catalysts aligns with the concept of waste-to-wealth in a sustainable society.

4. Conclusions

Overall, a facile and effective strategy has been developed to extract valuable metal resources from spent Mo–Ni/Al_2O_3 catalysts. Polymolybdic acid is primarily recovered in the form of coarse crystals with a small amount of ammonium molybdate, but its purity is equal to the commercially available molybdic acid. Alumina is also recovered in a high-purity, typical γ-Al_2O_3 phase. By utilizing recycled poly molybdic acid and pseudo-boehmite as raw materials, the prepared catalysts exhibit the same structure and dispersion of Mo species as the reference catalyst. Furthermore, these catalysts display comparative performance in denitrogenation, aromatic saturation, and hydrogenation to that of the reference catalyst, indicating a promising future for hydrogenation applications. This recycling technology for waste catalysts paves a solid path for sustainable development by transforming waste into wealth.

Table 2
Properties of resynthesized and reference catalyst applied in oil refinery

Crude oil and fraction	Sample #A'	Sample #R
Density (20 °C)/$g \cdot cm^{-3}$	0.9499	0.9464
Distillation range/°C	–	–
Initial boiling point (IBP)/(10%)	50/488	45/486
Viscosity (20 °C)/$mm^2 \cdot s^{-1}$	10.71	10.18
Carbon residue/%	0.02	0.02
Ash/%	<0.001	<0.001
Sulfur/$mg \cdot kg^{-1}$	27	33
Nitrogen/$mg \cdot kg^{-1}$	229	157
Carbon/%	89.08	89.35
Hydrogen/%	10.95	11.06
Aromatic carbon molar percentage/%	30.46	28.81
Hydrogen supply index/$mg \cdot g^{-1}$	0.228	0.232
Mass spectrum (MS)/%		
Alkanes	3.4	3.3
Total cycloparaffins	31.8	37.0
Total aromatics	64.8	59.7
Resins	0	0

Declaration of Interest

The authors declare that they have no known competing financial interests or personal relationships that could have appeared to influence the work reported in this paper.

Acknowledgements

This work was supported by grants from the National Key Research and Development Program of China (2023YE41507601), the National Natural Science Foundation of China (22122807, 22378038), the Fundamental Research Funds for the Central Universities (DUT23RC(3)044), and State Key Laboratory of Heavy Oil Processing, China University of Petroleum (WX20230149).

Supplementary Material

Supplementary data to this article can be found online at https://doi.org/10.1016/j.cjche.2024.01.006.

Nomenclature

L	average slab length of MoS_2, nm
L_i	slab length of the ith MoS_2 unit, nm
N	stacking layer number of MoS_2
N_i	stacking layer number of the ith MoS_2
S_i	number of slabs or stacks in a determined range of the ith MoS_2
θ	half angle between the incident X-ray and its diffraction, (°)

References

[1] H.M. Sun, J.T. Yang, H.W. Zhang, Q. Yang, S.Z. Wu, Y.X. Wang, H.B. Zhu, Y.Y. Yue, T.H. Wang, P. Yuan, Hierarchical flower-like NiCu/SiO_2 bimetallic catalysts with enhanced catalytic activity and stability for petroleum resin hydrogenation, *Ind. Eng. Chem. Res.* 60 (15) (2021) 5432–5442.
[2] J.J. Li, Z.Q. Zhang, G.F. Qin, X.D. Tang, C.X. Xiang, Fe/HZSM-5 catalytic pyrolysis cellulose as hydrogen donor for the upgrading of heavy crude oil by one-pot process, *Fuel* 298 (2021) 120880.
[3] R. Saab, K. Polychronopoulou, L.X. Zheng, S. Kumar, A. Schiffer, Synthesis and performance evaluation of hydrocracking catalysts: A review, *J. Ind. Eng. Chem.* 89 (2020) 83–103.
[4] M. Marafi, A. Stanislaus, Spent catalyst waste management: A review, *Resour. Conserv. Recycl.* 52 (6) (2008) 859–873.
[5] H. Al-Sheeha, M. Marafi, V. Raghavan, M.S. Rana, Recycling and recovery routes for spent hydroprocessing catalyst waste, *Ind. Eng. Chem. Res.* 52 (36) (2013) 12794–12801.
[6] A. Tanimu, K. Alhooshani, Advanced hydrodesulfurization catalysts: A review of design and synthesis, *Energy Fuels* 33 (4) (2019) 2810–2838.
[7] S. Bag, A.F. Gaudette, M.E. Bussell, M.G. Kanatzidis, Spongy chalcogels of non-platinum metals act as effective hydrodesulfurization catalysts, *Nat. Chem.* 1 (3) (2009) 217–224.
[8] Y.C. Lai, W.J. Lee, K.L. Huang, C.M. Wu, Metal recovery from spent hydrodesulfurization catalysts using a combined acid-leaching and electrolysis process, *J. Hazard Mater.* 154 (1–3) (2008) 588–594.
[9] H. Wu, S.Y. Duan, D.D. Liu, X.F. Guo, A.F. Yi, H.R. Li, Recovery of nickel and molybdate from ammoniacal leach liquor of spent hydrodesulfurization catalyst using LIX84 extraction, *Sep. Purif. Technol.* 269 (2021) 118750.
[10] M. Marafi, A. Stanislaus, Waste catalyst utilization: Extraction of valuable metals from spent hydroprocessing catalysts by ultrasonic-assisted leaching with acids, *Ind. Eng. Chem. Res.* 50 (16) (2011) 9495–9501.
[11] N.M. Al-Mansi, M.N.M. Abdel, Recovery of nickel oxide from spent catalyst, *Waste Manag.* 22 (1) (2002) 85–90.
[12] J.L. Liu, C.Y. Wang, X.R. Wang, C. Zhao, H.Q. Li, G.Y. Zhu, J.B. Zhang, Reconstruction and recovery of anatase TiO_2 from spent selective catalytic reduction catalyst by NaOH hydrothermal method, *Chin. J. Chem. Eng.* 60 (2023) 53–60.
[13] S.P. Barik, K.H. Park, P.K. Parhi, J.T. Park, C.W. Nam, Extraction of metal values from waste spent petroleum catalyst using acidic solutions, *Sep. Purif. Technol.* 101 (2012) 85–90.
[14] J.Z. Wang, S.N. Wang, A. Olayiwola, N. Yang, B. Liu, J.J. Weigand, M. Wenzel, H. Du, Recovering valuable metals from spent hydrodesulfurization catalyst *via* blank roasting and alkaline leaching, *J. Hazard Mater.* 416 (2021) 125849.
[15] G.H. Li, D.P. Shi, H. Sun, Q.Z. Bu, J. Luo, M.J. Rao, Z.W. Peng, T. Jiang, Effects and mechanisms of ternary solution of NaOH-Na_2CO_3-Na_2SO_4 on the recovery of molybdenum from residues containing multiple molybdates, *Sep. Purif. Technol.* 248 (2020) 117059.
[16] S.J. Zhao, Z.Q. Liao, Y. Xie, X.S. Li, Y.Y. Dai, Z.R. Li, M.Y. Wang, Extraction of molybdenum from spent HDS catalyst by pressure alkaline leaching, *J. Sustain. Metall.* 7 (3) (2021) 773–782.
[17] Y.W. Wang, Z.Q. Wang, J.J. Huang, Y.T. Fang, Improved catalyst recovery combined with extracting alumina from Na_2CO_3-catalyzed gasification ash of a high-aluminium coal char, *Fuel* 234 (2018) 101–109.
[18] M. Marafi, M.S. Rana, H. Al-Sheeha, The Recovery of Valuable Metals and Recycling of Alumina from a Waste Spent Hydroprocessing Catalyst: Extraction with Na salts WIT Transactions on Ecology and the Environment, Waste Management and the Environment VII. Ancona, Italy, WIT Press, Southampton, UK, 2014.
[19] E. Kordouli, B. Pawelec, K. Bourikas, C. Kordulis, J.L.G. Fierro, A. Lycourghiotis, Mo promoted Ni-Al_2O_3 co-precipitated catalysts for green diesel production, *Appl. Catal. B Environ.* 229 (2018) 139–154.
[20] A. Siahvashi, D. Chesterfield, A.A. Adesina, Nonoxidative and oxidative propane dehydrogenation over bimetallic Mo–Ni/Al_2O_3 catalyst, *Ind. Eng. Chem. Res.* 52 (11) (2013) 4017–4026.
[21] L. Qu, C.T. Li, G.M. Zeng, M.Y. Zhang, M.F. Fu, J.F. Ma, F.M. Zhan, D.Q. Luo, Support modification for improving the performance of MnO_x–CeO_y/γ-Al_2O_3 in selective catalytic reduction of NO by NH_3, *Chem. Eng. J.* 242 (2014) 76–85.
[22] J.M. Rynkowski, T. Paryjczak, M. Lenik, On the nature of oxidic nickel phases in NiO/γ-Al_2O_3 catalysts, *Appl. Catal. Gen.* 106 (1) (1993) 73–82.
[23] C. Volkringer, H. Leclerc, J.C. Lavalley, T. Loiseau, G. Férey, M. Daturi, A. Vimont, Infrared spectroscopy investigation of the acid sites in the metal–organic framework aluminum trimesate MIL-100(Al), *J. Phys. Chem. C* 116 (9) (2012) 5710–5719.
[24] A. Travert, C. Dujardin, F. Maugé, E. Veilly, S. Cristol, J.F. Paul, E. Payen, CO adsorption on CoMo and NiMo sulfide catalysts: A combined IR and DFT study, *J. Phys. Chem. B* 110 (3) (2006) 1261–1270.
[25] K. Hadjiivanov, H. Knözinger, M. Mihaylov, FTIR study of CO adsorption on Ni–ZSM-5, *J. Phys. Chem. B* 106 (10) (2002) 2618–2624.
[26] B.M. Vogelaar, N. Kagami, T.F. van der Zijden, A.D. van Langeveld, S. Eijsbouts, J.A. Moulijn, Relation between sulfur coordination of active sites and HDS activity for Mo and NiMo catalysts, *J. Mol. Catal. Chem.* 309 (1–2) (2009) 79–88.
[27] Q.Y. Zhao, X.L. Hou, J.L. Wang, D.G. Cheng, F.Q. Chen, X.L. Zhan, Engineering specific Mo–O bond stretching to activate lattice oxygen in V-doped Bi_2MoO_6 for enhanced oxidative dehydrogenation of 1-butene, *Ind. Eng. Chem. Res.* 62 (1) (2023) 329–340.
[28] C.I. Vargas-Consuelos, M.A. Camacho-López, V.H. Ramos-Sanchez, O.A. Graeve, Phase and morphology control of hexagonal MoO_3 crystals *via* Na^+ interactions: A Raman spectroscopy study, *J. Phys. Chem. C* 127 (27) (2023) 13136–13148.
[29] B. Courcot, A.J. Bridgeman, Structural and vibrational study of $[Mo_7O_{24}]^{6-}$ and $[W_7O_{24}]^{6-}$, *J. Phys. Chem. A* 113 (39) (2009) 10540–10548.
[30] W.G. Klemperer, W. Shum, Synthesis and interconversion of the isomeric. alpha.- and.beta.-molybdate ($Mo_8O_{26}^{4-}$) ions, *J. Am. Chem. Soc.* 98 (25) (1976) 8291–8293.
[31] C.H. Liu, Q. Wei, Y.S. Zhou, X.Y. Liu, K.X. Deng, W.B. Huang, H.R. Liu, Z.Q. Yu, A study on the role of Ti/Si atomic ratios in the hydrodenitrogenation activity of NiMo/TiO_2-SiO_2 catalyst, *Fuel* 338 (2023) 126922.
[32] A. Karmakar, K. Karthick, S.S. Sankar, S. Kumaravel, M. Ragunath, S. Kundu, Oxygen vacancy enriched $NiMoO_4$ nanorods *via* microwave heating: A promising highly stable electrocatalyst for total water splitting, *J. Mater. Chem. A* 9 (2021) 11691–11704.